Mar Syst Ocean Technol (2015) 10:71–90
DOI 10.1007/s40868-015-0007-2

# Fundamental green water study for head, beam and quartering seas for a simplified FPSO geosim using a mixed experimental and numerical approach

**Felipe Ruggeri[1] · Rafael A. Watai[1] · Pedro Cardozo de Mello[1] · Claudio Mueller P. Sampaio[1] · Alexandre N. Simos[1] · Daniel Fonseca de Carvalho e Silva[2]**

Received: 16 December 2014 / Accepted: 28 May 2015 / Published online: 13 June 2015


**Abstract** The prediction of green water events on FPSO is very important from both the design and operational point of view, requiring the development of a specific methodology regarding the problem. The computation of the loads on structures located on the main deck in the design stage is important to define reinforcements in the equipments to avoid damages. Besides, the freeboard prediction is important to define the operational windows and limit conditions since the deck activities should be interrupted if there is a risk of overtopping. Since it is unfeasible to perform an extensive experimental campaign regarding all the sea states verified in the operational site, the use of numerical methods is often considered. In order to verify the accuracy of the numerical results, an experimental campaign is performed regarding a simplified FPSO geometry and the results are compared with both BEM and FVM computations to validate the numerical results. This article compares the results regarding the captive model test (i.e., body motions are absent) which will be complemented in a next article regarding the floating body in waves.

**Keywords** Green water · FPSO · Deck loads

✉ Felipe Ruggeri
felipe.ruggeri@gmail.com; fauthor@example.com

[1] Department of Naval Architecture and Ocean Engineering, University of São Paulo, São Paulo, Brazil

[2] CENPES - Petrobrás S.A., Rio de Janeiro, Brazil

## 1 Introduction

The recent discoveries of oil reservoir in the pre-salt layer of Santos basin provided new challenges to the Brazilian offshore industry due to the deep waters and harsh environmental conditions compared with the Campos one. The offshore units most used in the Brazilian coast for oil extraction and production are FPSOs,[1] ships converted to oil platforms or built from zero to this purpose, always keeping a ship shape. Under severe wave conditions, this kind of platform is subjected to green water event, a solid mass of water that overtops the freeboard and propagate in the deck, reaching topside equipments and structures, which can provide damage and increase the operation downtime. According to [9], green water events have become a growing concern to the offshore industry and several incidents over the last years were reported by [5] that happened under conditions considerably below the centenary ones. The definition of loads in these equipments and structures located in the topside is very important in the design stage to improve the position and protections that are added to avoid damages in the equipments. Besides, the definition of the most susceptible conditions to green water events is important for the schedule of the crew activities in the main deck.

The importance of the problem motivated several studies, for instance the JIP SafeFlow which used both experimental and numerical approaches to the problem with a good overview provided by [1], among them the Glim's method with shallow water equations concerning water on deck and nonlinear time domain rankine panel method to provide the boundary conditions required [2, 12].

[1] Floating production storage and offloading.

In additional [1] states the stages of green water events as the freeboard exceedance prediction, water on deck propagation and loadings (pressures) in the structures located in the topside.

There are several studies in the literature concerning green water events under head sea conditions, mainly because in several locations the platforms are moored by SPM[2] using a turret structure, which allows the unit to be aligned with the net force acting in the hull. One of the major concerns under this condition is the integrity of the turret, since it provides weathervaning capability and is an expensive equipment. Although the platform is headed to this net force vector, which can be affected by wind and current, the platform will be almost all the time headed to the waves under a severe sea state condition, which can provide water in deck in the fore region; therefore, a lot of mitigating devices are applied in the fore region (i.e., fore castle). However, a significant amount of oil platforms in the pre-salt region will use a spread mooring system with the benefit of saving costs associated with turret acquisition/maintenance. On the other hand, the hull becomes more exposure to beam and bow/stern quartering sea conditions in which the green water phenomena have not being deeply investigated in the literature. The study of green water in such conditions is a challenge for the engineers, since there are no well-established procedures available and ready to use in the early stage of the design. Actually most of the rules available for design neglect green water events under beam sea conditions.

It should be noticed that there is an inherent complexity associated with nonlinear hydrodynamic effects, especially concerning the wave run-up along the FPSO bow and sidehull since the hull structures above the water plane interact with the incident wave field.

Besides, under beam seas the roll motions are appreciably nonlinear and the definition of the critical conditions is difficult because relative motions concerning the freeboard change with both wave run-up, more intense for short waves, and roll motions, with higher amplitudes for long periods. The relative phases between motions and free surface elevation are also very important close to resonance because the phases can shift up to 180°.

The use of numerical methods combined with experimental tests for hydrodynamic studies has become very common in the last years, allowing designers to validate numerical predictions with experimental data and then extrapolate the results for several additional conditions. This methodology is very important because the simulation of the entire metocean conditions of an offshore location is unfeasible following an experimental approach. Although several numerical codes that solve Navier-Stokes equations combined to the continuity one have been developed recently, it's use for seakeeping analysis still a challenge due to the free surface effects and body–fluid interactions. The experimental approach was performed assuming Froude (or KC) similarity, therefore assuming that viscous effects do not change with model scale in green water/impact problems, which is also a fundamental hypothesis for potential flow theory.

Following this approach, some simplified methodologies were developed for initial design stages such as KINEMA, described in [11], which considers the body dynamics as linear neglecting the effect of water on deck with some validation cases for irregular waves discussed in [8]. The motions are computed transposing the results from frequency to time domain following [3], assuming only some corrections in the incident wave field kinematics in the computation of the relative elevation. This relative free surface elevation combined to the velocity field provides the boundary conditions to modified dam-break theories for the computation of water on deck propagation. However, it should be noticed that [1] states that water on deck can change the body dynamics, which is a complex nonlinear effect to be considered in the numerical simulation using potential theory. Besides, since green water events are usually considered for high steepness waves, the body response can become nonlinear regardless the water on deck, see for instance the roll motions increasing wave steepness. Therefore, it is really difficult to define the influence of water on deck and pressure/velocity field nonlinearities. This study is focused on the pre-salt layer sea state conditions that are appreciably less severe than North Sea ones, motivating an experimental campaign and comparison to numerical simulations to verify the influence of nonlinear effects.

Additionally, the study is also focused on the validation of numerical methods with experimental data to verify the capability to predict the trends and also the accuracy of the computations. An extensive experimental campaign was conducted in the Hydrodynamic Calibrator of the Numerical Offshore Tank of the University of Sao Paulo to provide a validation database of numerical methods.

The quantities measured in the experiments were wave elevation along the FPSO sidehull (run-up) and above the deck, forces and pressure on blocks located in the deck and the platform motions. These tests were recorded by four video cameras, two of them attached to the model to simplify the phenomenon analysis and comprehension in complex situations, such as water splashing and wave breaking. A collection of six different model arrangements was tested considering both fixed (captive) and moored vessel under head (180°), bow quartering (225°) and beam seas condition (270°). A total of 14 regular were performed for a single draft (full loaded) condition, which was

[2] Single Point Mooring.

assumed as the most critical configuration for green water events. Since the main goal was to provide a database for numerical model validation, severe conditions were selected in order to increase water on deck and loads. The model was built without most of the appendages to simplify the numerical methods comparison (i.e., riser balcony, forecastle, bulwark, deckhouse, etc). This is also a fundamental hypothesis for a frequency domain potential flow estimative since the method neglects the geometry above the waterline. However, it should be noticed that the hull geometry above the waterline can change the free surface elevation pattern due to nonlinear interactions, mainly for a non-vertical wall-sided model.

The numerical comparisons were split in two stages: prediction of the free surface elevation around the hull using potential flow theory and finite volume method computations, the last one also applied in the comparison of impact forces on load cells located on deck. In order to simplify the analysis, the first results analyzed were based on captive model tests in order to simplify the computations since the body motions do not need to be computed.

## 2 Experimental setup

The tests were performed in the Hydrodynamic Calibrator (CH-TPN) of the Numerical Offshore Tank of the University of Sao Paulo, a squared 14 × 14 m wave basin with 4.1 m of water depth equipped with 148 active flap-type wave makers, each one connected to a wave probe, providing the simultaneous wave generation and absorption capability, as described in [6].

The model was manufactured in naval plywood and polyurethane, the first one in the parallel middle body and the later in the aft and fore regions under a 1/100 scale as can be seen in Fig. 1. The hull geometry main dimensions and properties are shown in Table 1.

**Fig. 1** Model constructed in plywood and polyurethane

**Table 1** Model main dimensions and properties

| Parameter | Full scale | Model scale | Unit |
|---|---|---|---|
| Length overall (LOA) | 288.0 | 2.88 | m |
| Beam ($B$) | 54.0 | 0.54 | m |
| Depth ($D$) | 31.0 | 0.31 | m |
| Draft ($T$) | 23.0 | 0.23 | m |
| Displacement ($\Delta$) | 350.907 | 0.350 | Ton |

The first stage of green water is the freeboard exceedance, which is required (but not sufficient) to guarantee water on deck [13], so the relative free surface elevation was measured by a collection of 9 wave probes located close to the sidehull, as shown in Fig. 2 with the positions shown in Table 2, assuming a coordinate system with origin located amidship in the plane of symmetry on the deck level. The x-coordinate is positive toward the bow, the y-direction positive in portside, and z-direction positive upward. The probe measurement capacity was in the range of ±20 cm (model scale or ±20 m in real scale) from the undisturbed free surface level.

In order to measure the impact forces, four blocks attached to load cells were positioned on the deck in the positions presented in Table 2. It should be noticed that load cells FA02, FA03 and FA04 were kept aligned with $y$-axis direction during all simulations while load cell FA01

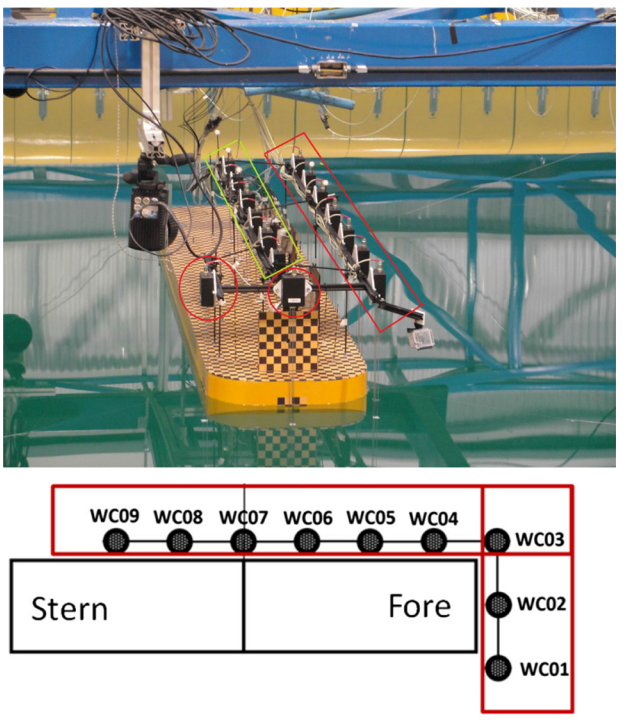


**Fig. 2** Wave probe position along the sidehull (in *red*) (Color figure online)

**Table 2** Sidehull wave probes and load cell position

| Type | Name | Real $X$ (m) | Scale $Y$ (m) | Model $X$ (m) | Scale $Y$ (m) |
|---|---|---|---|---|---|
| Wave probe | WC01 | 140.0 | −27.0 | 1.40 | −0.27 |
| Wave probe | WC02 | 144.0 | 0.0 | 1.44 | 0.00 |
| Wave probe | WC03 | 140.0 | 27.0 | 1.40 | 0.27 |
| Wave probe | WC04 | 105.0 | 27.0 | 1.05 | 0.27 |
| Wave probe | WC05 | 70.0 | 27.0 | 0.70 | 0.27 |
| Wave probe | WC06 | 35.0 | 27.0 | 0.35 | 0.27 |
| Wave probe | WC07 | 0.0 | 27.0 | 0.00 | 0.27 |
| Wave probe | WC08 | −35.0 | 27.0 | −0.35 | 0.27 |
| Wave probe | WC09 | −70.0 | 27.0 | −0.70 | 0.27 |
| Load cell | FA01 | 134.0 | 0.0 | 1.34 | 0.00 |
| Load cell | FA02 | 74.0 | 17.0 | 0.74 | 0.17 |
| Load cell | FA03 | 4.9 | 17.0 | 0.05 | 0.17 |
| Load cell | FA04 | −66.0 | 17.0 | −0.66 | 0.17 |

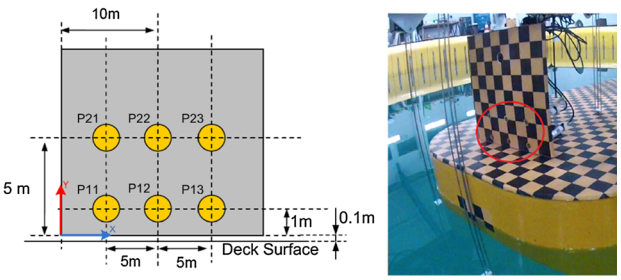


**Fig. 3** Pressure gauges and load cells used in the model test

(located in the fore region) was aligned with x-direction in the 0° and 225° conditions and with y-direction in the 270°, assuming that these directions would amplify the forces. The dimensions concerning the load cells can also be seen in Fig. 3.

The load cell nominal ranges were 20N (model scale) for FA02 and FA04 and 50N (model scale) for FA01 and FA03 (model scale) under a sampling rate of 100 Hz due to acquisition constrains. Although the force "peak" during the impact rise time could not be captured completely, the global impact force could be measured. However, it should also be noticed that the FVM[3] simulations performed could not capture the force "peak" due to limitations in terms of computational effort, which is presented in Sect. 3.

The natural frequency of the block forces with load cells FA02, FA03 and FA04 was about 60 Hz (model scale) while the impact block containing load cell FA01 was 26.35 Hz measured from decay tests.

The regular waves selected can be seen in Table 3. Although the results presented in this first work are based on the captive model test, the waves were selected based on the natural periods of the model, since body motions (including phases) are very important to green water events [1]. The regular waves 01–03 are close to the roll natural period, waves 04, 10R, 11 are between roll and heave natural periods, wave 05 is a very long period, waves 06–08 and 12 are between heave and pitch natural periods, and waves 09 and 09R are below pitch natural periods. In order to verify the influences of nonlinearities, the waves were generated assuming several wave heights for the same periods, providing different wave steepness.

## 3 Analysis, comparison with numerical methods and results

The experimental data were analyzed to obtain the free surface elevation around the hull and forces on the blocks located on deck. The wave run-up was evaluated using WAMIT first-order module, which is based on frequency domain potential theory (more details can be verified in [4]). By hypothesis the linear potential predictions should provide good estimations for low steepness waves under low KC[4] numbers. In this theory the free surface is described as mathematical function; thus, there is no possibility of overturning waves or wave breaking (see for instance [7]), and the computation become more accurate as the low steepness, low incident wave amplitude and low KC number are achieved. However, it is well known and verified experimentally that this theory goes beyond its hypothesis providing good estimations for initial phases of design. Actually even when the results are not so accurate, the method still predicting most of trends related to the problem, which can be applied to define critical conditions

[3] Finite volume methods.

[4] Keulegan carpenter.

**Table 3** Regular generated waves

| ID | Type | Real $T$ (s) | Scale $H$ (m) | Model $T$ (s) | Scale $H$ (m) | $\epsilon$ (%) |
|---|---|---|---|---|---|---|
| Reg01 | Regular | 17.5 | 10.5 | 1.75 | 0.105 | 2.2 |
| Reg02 | Regular | 17.5 | 12.5 | 1.75 | 0.125 | 2.6 |
| Reg03 | Regular | 17.5 | 15.0 | 1.75 | 0.150 | 3.1 |
| Reg04 | Regular | 15.0 | 12.5 | 1.50 | 0.125 | 3.6 |
| Reg05 | Regular | 20.0 | 12.5 | 2.00 | 0.125 | 2.0 |
| Reg06 | Regular | 12.5 | 12.5 | 1.25 | 0.125 | 5.1 |
| Reg07 | Regular | 12.5 | 10.5 | 1.25 | 0.105 | 4.3 |
| Reg07R | Regular | 12.5 | 7.0 | 1.25 | 0.070 | 2.9 |
| Reg08 | Regular | 12.5 | 15.0 | 1.25 | 0.150 | 6.2 |
| Reg09 | Regular | 11.5 | 12.5 | 1.15 | 0.125 | 6.1 |
| Reg09R | Regular | 10.0 | 7.0 | 1.00 | 0.070 | 4.5 |
| Reg10R | Regular | 15.0 | 10.5 | 1.50 | 0.105 | 3.0 |
| Reg11 | Regular | 15.0 | 20.0 | 1.50 | 0.200 | 5.7 |
| Reg12 | Regular | 12.5 | 20.0 | 1.25 | 0.200 | 8.2 |

to be checked through experimental approach or more complex numerical methods.

However, the frequency domain potential method cannot evaluate the effects above the waterline because the problem is solved at the undisturbed free surface; therefore, the forces on structures located in the topside must be evaluated by a different method. The FVM was chosen to evaluate the forces on structures located on the topside, also providing the wave run-up around the hull.

### 3.1 Free surface elevation comparisons

#### *3.1.1 Potential flow computations*

The initial study was conducted using the software WAMIT, a frequency domain boundary element method, considering only the first-order (linear) solution. The numerical method used allows two kinds of solution/geometry description, a low-order method that considers the geometry described by flat triangular/quadrilateral panels with all quantities (potential, pressure, velocity, etc.) constant inside each element, and a higher-order approach that considers the geometry "exactly" using the spline description, as the quantities over the elements. Since the higher-order approach guarantees more accurate results for the same number of elements used in the low-order method, the first one was adopted in WAMIT simulations.

An illustration of the geometry assumed in WAMIT can be seen in Fig. 4, considering only the mean wetted surface.

In order to obtain a description concerning the free surface elevation around the hull, a grid point of 720 elements was evaluated, considering the points shown in Fig. 5. The evaluation of free surface elevation was performed considering only the elevation magnitude, since for the fixed hull the phase is unimportant in the prediction of freeboard exceedance without any additional consideration about the flow direction and velocity components.

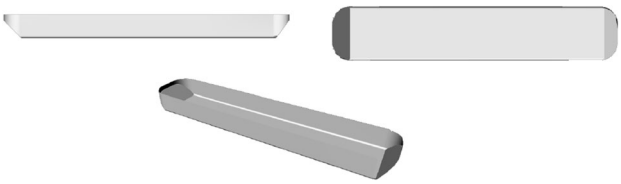

**Fig. 4** Platform geometry considered in WAMIT

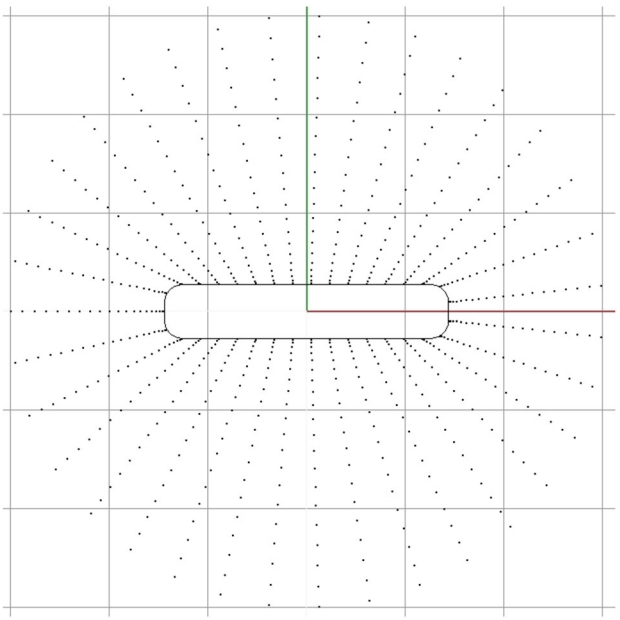

**Fig. 5** Grid points for free surface elevation evaluation in WAMIT

In order to guarantee the correct evaluation of free surface elevation, a convergence analysis was performed

considering WAMIT results, changing the panel size, a parameter that controls the number of elements in the higher-order method. The analysis was focused on the first layer of panels near the hull (about 1 cm distant from the hull in model scale, 1m in full scale), where the free surface elevation would be more relevant in the prediction of freeboard exceedance. The panel size values chosen for this study were 0.5, 0.25 and 0.125, obtaining the results shown in Figs. 6, 7 and 8 for headings 180, 225 and 270, respectively.

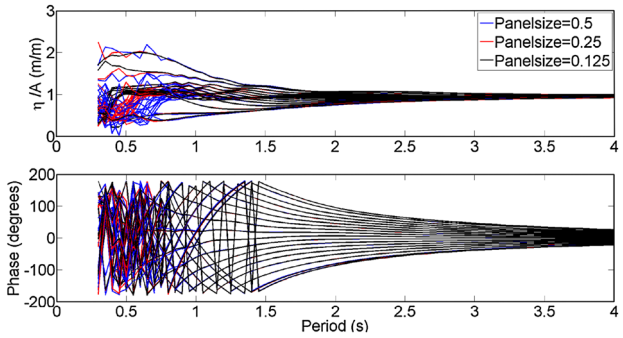


**Fig. 6** Convergence analysis for free surface elevation considering only the first layer of grid points, heading 180 (Color figure online)

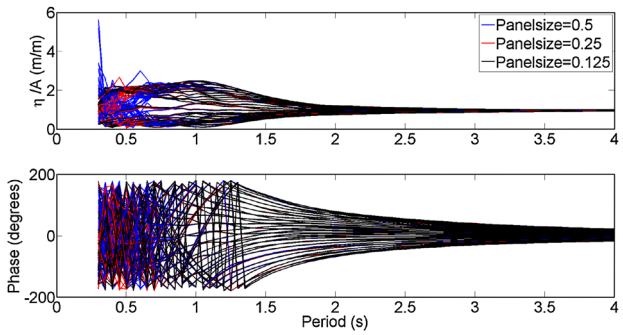


**Fig. 7** Convergence analysis for free surface elevation considering only the first layer of grid points, heading 225 (Color figure online)

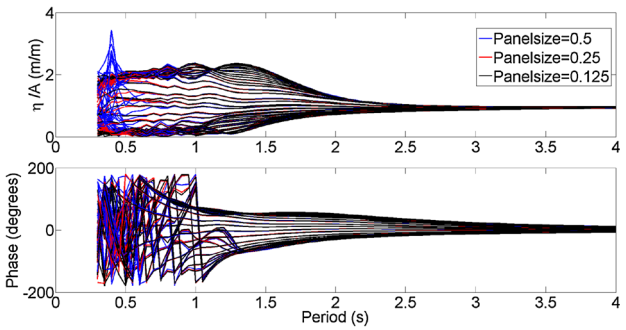


**Fig. 8** Convergence analysis for free surface elevation considering only the first layer of grid points, heading 270 (Color figure online)

Although the relative phase between free surface elevation and the incident wave is less important in this first analysis compared with the floating case, the convergence analysis focused on both module and phase, since a next step in the study would be the application of some additional corrections concerning the flow velocity, a condition that makes the relative phase very important. It should be noticed from the numerical results that for all the waves experimentally tested (above 1.0 s in model scale, 10 s in real scale) the agreement is remarkable for both module and phase. However, as the wave length decreases (mainly bellow 0.6 s), there are considerable variations, which was expected because the shorter the waves are, the smaller the panel must be to correctly compute the flow characteristics.

In order to evaluate the free surface elevation convergence considering all points in the free surface for wave periods higher than 1.0 s (model scale), the differences between free surface elevation concerning the two finest meshes were calculated, as the phase difference, which is shown in Figs. 9, 10 and 11, where the black line limits the points closer to the hull and each color denotes a wave period. It can be seen that the differences concerning all points are less than 1.5 % for free surface elevation and less than 3° for relative phases considering the points

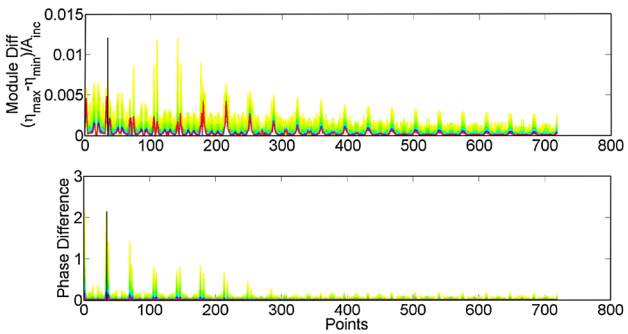


**Fig. 9** Convergence analysis for free surface elevation considering all grid points for wave periods higher than 1.0 s, heading 180, fixed model

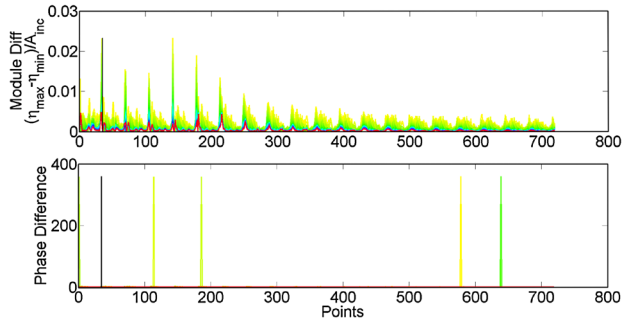


**Fig. 10** Convergence analysis for free surface elevation considering all grid points for wave periods higher than 1.0 s, heading 225, fixed model

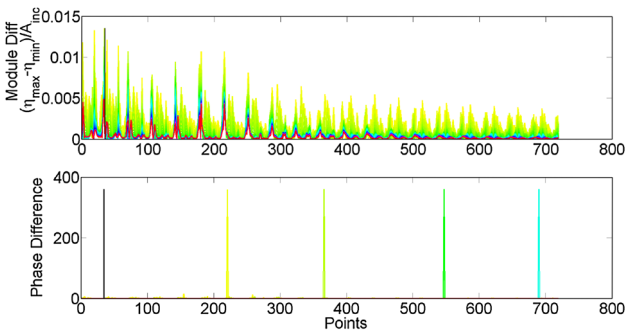


**Fig. 11** Convergence analysis for free surface elevation considering all grid points for wave periods higher than 1.0 s, heading 270, fixed model

placed in the first layer of grid points. So the numerical results obtained using the finest mesh (panel size = 125) were judged fine to be used in the numerical evaluation of freeboard exceedance and comparison with experimental results.

### 3.1.2 *Comparison between numerical predictions and experimental results*

In order to validate the numerical model, several comparisons were performed, obtaining a fine agreement for almost all condition, even for the high steepness waves. The analysis was performed based on the sidehull wave probe time series, comparing the maximum/minimum values with the absolute amplitude predicted by WAMIT.

It was verified that even for the high steepness waves, although the experimental signal shape was not sinusoidal/regular, the amplitude (maximum value) is still in good agreement with the numerical estimation, especially for the wave crests, as can be seen, for example, in Fig. 12 for the

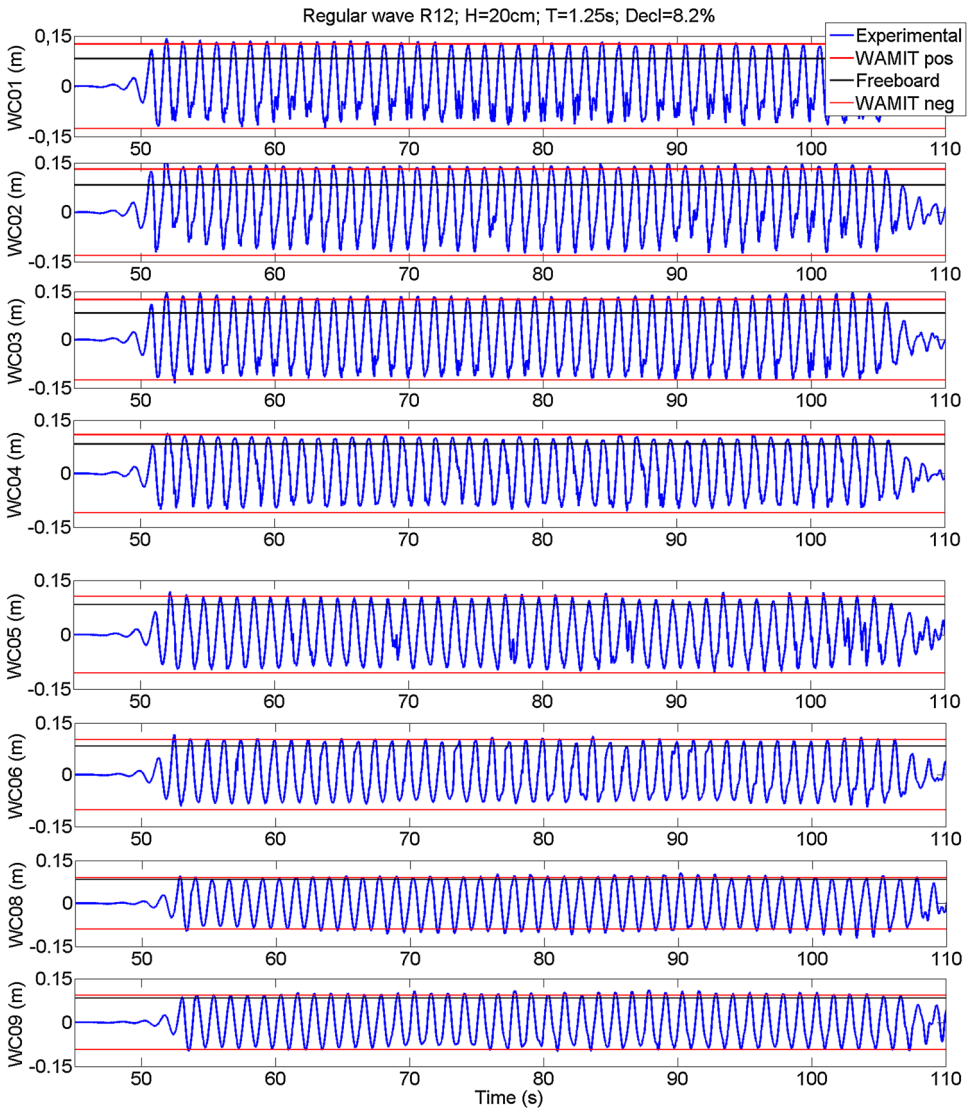


**Fig. 12** Comparison of wave run-up between experimental test and numerical prediction for high steepness wave for heading 180, fixed model (model scale) (Color figure online)

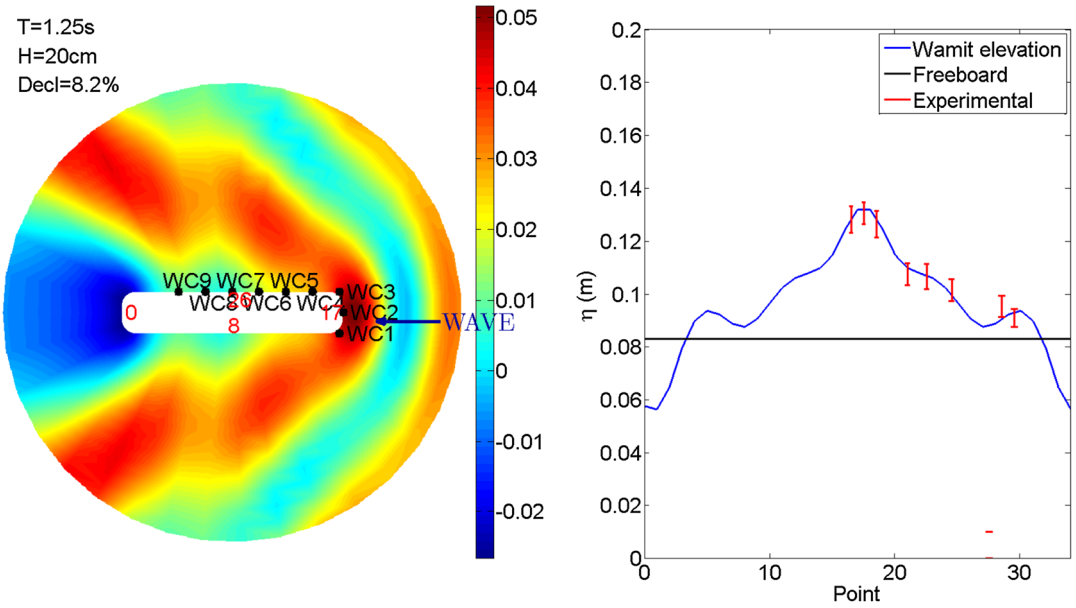


**Fig. 13** Comparison of experimental test (*blue line*) and numerical prediction (*red dots*) for high steepness wave for heading 180, fixed model (model scale) (Color figure online)

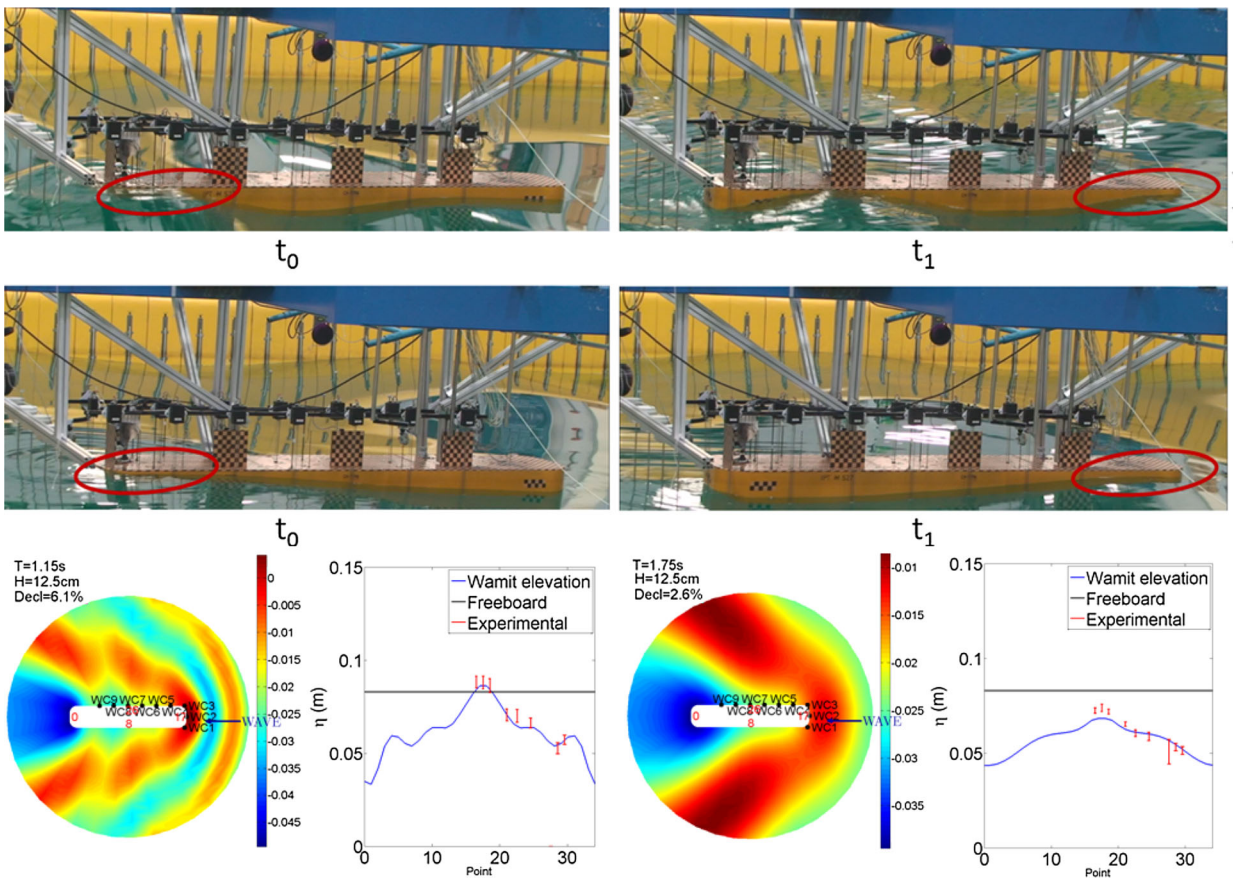


**Fig. 14** Comparison of a short wave ($T = 1.15$ s, $\lambda = 2.06$ m—model scale/ $T = 11.5$ s, $\lambda = 206$ m—real scale) and long wave ($T = 1.75$ s, $\lambda = 4.78$ m—model scale/$T = 17.5$ s, $\lambda = 478$ m—real scale) with the same wave height ($H = 12.5$ cm—model scale/$H = 12.5$ m—real scale), considering both experimental test and numerical predictions for heading 180, fixed model (Color figure online)

highest steepness tested. It should be noticed that for all the sidehull wave probes the wave crest maximum values could be evaluated properly, but the wave through could not be predicted so well because the green water events make difficult the probe measurements, since part of the water that overtops the freeboard crashes into the force block and comes back to the probe. The free surface elevation maps can be seen, for example, in Fig. 13 that shows the sidehull wave probe location, as the free surface elevation for the first layer of the grid points (near the hull). The red numbers in the hull picture show some of the points in the first layer of the grid points in order to orient the free surface amplitude considering the black line as the freeboard. The figure on right shows the comparison between WAMIT predictions (blue continuous line) and experimental data (red bars) in the wave probe position. It should be noticed that a error bar is created based on amplitude fluctuations during the several wave cycles in the experimental test, which can also be verified in Fig. 12.

### 3.2 Experimental observations supported by the numerical computations

The results concerning numerical simulations provided the background to better comprehend the experimental data for the several wave directions, as described next.

#### *3.2.1 180 degrees heading*

As already pointed out, the head sea condition is one of the most studied concerning green water events for floating bodies, either with or without forward speed. However, there are not a large number of publications concerning the captive model situation, a situation without radiated waves.

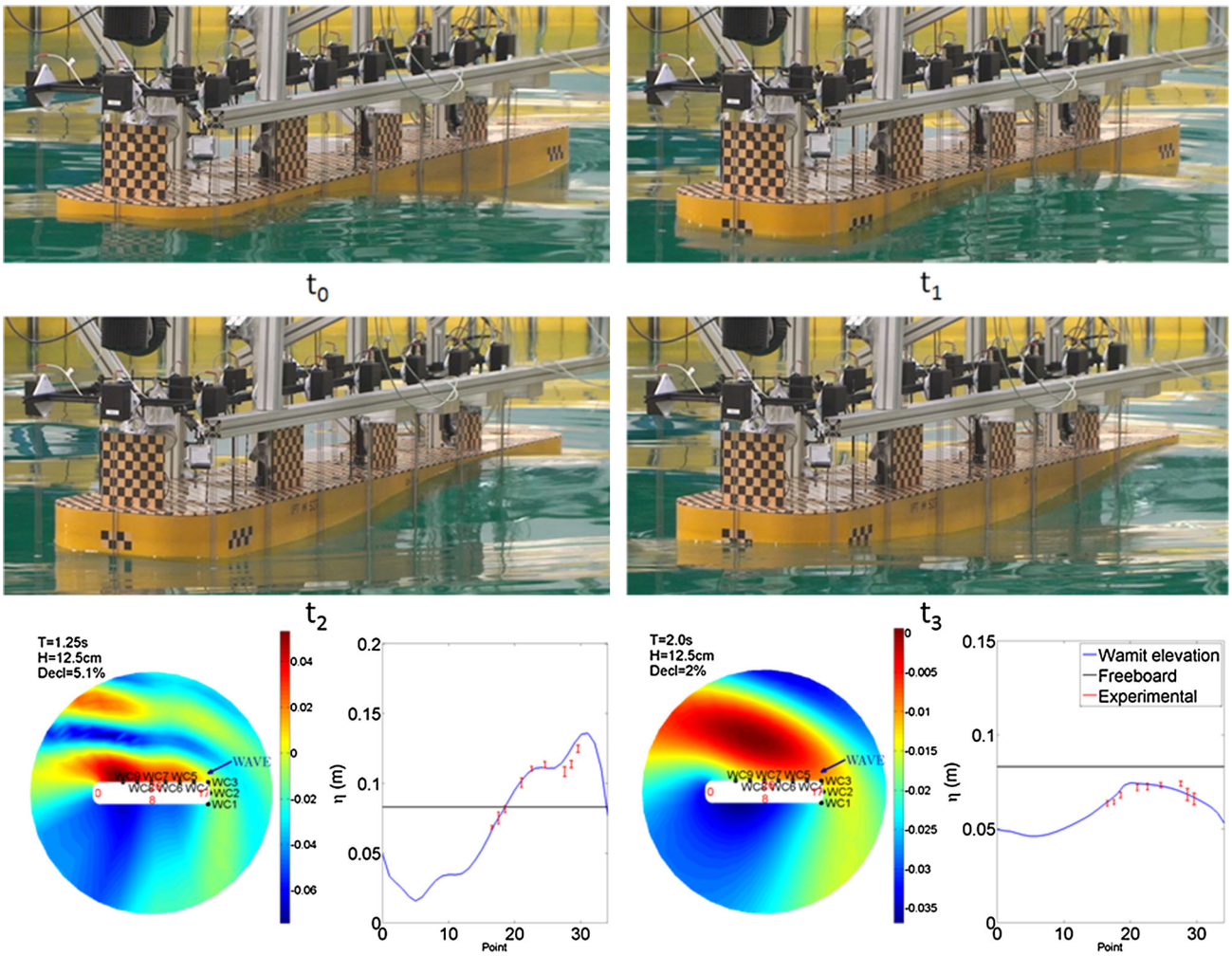


**Fig. 15** Comparison of a short wave ($T = 1.25$ s, $\lambda = 2.43$ m—model scale/$T = 12.5$ s, $\lambda = 243$ m—real scale) and long wave ($T = 2.00$ s, $\lambda = 6.25$ m—model scale/$T = 20.0$ s, $\lambda = 625$ m—real scale) with the same wave height ($H = 12.5$ cm—model scale/$H = 12.5$ m—real scale), considering both experimental test and numerical predictions for heading 225, fixed model (Color figure online)

The experimental tests performed and numerical simulations showed a similar behavior concerning the waves analyzed, regardless the wave length/period. In head seas there is always a higher free surface elevation near the fore region that reduces toward the stern region, reducing the probability of green events amidship or in the stern, since the freeboard exceedance does not happen for most of the situations. The comparison concerning a short wave ($T = 1.15$ s, $\lambda = 2.06$ m—model scale/$T = 11.5$ s, $\lambda = 206$ s—real scale) and long wave ($T = 1.75$ s, $\lambda = 4.78$ m—model scale/$T = 17.5$ s, $\lambda = 478$ m—real scale) can be seen in Fig. 14. It can be verified that although both waves have the same height of 12.5 cm (model scale), the diffraction effects in the shorter are sufficient to guarantee an accumulation of water in the fore region, providing green water events, while in the long wave it does not happen. This effect could also be verified in the numerical analysis performed using WAMIT linear model, as can be seen in the elevation map and free surface elevation plot, that predicted the freeboard exceedance for the short wave and not for the longer one, even with the short wave containing 6.1 % of wave steepness, which could introduce some nonlinear effects.

### 3.2.2 225 degrees heading

The analysis concerning the 225° verified that for short waves ($T = 1.25$ s, $\lambda = 2.44$ m—model scale/ T=12.5s,

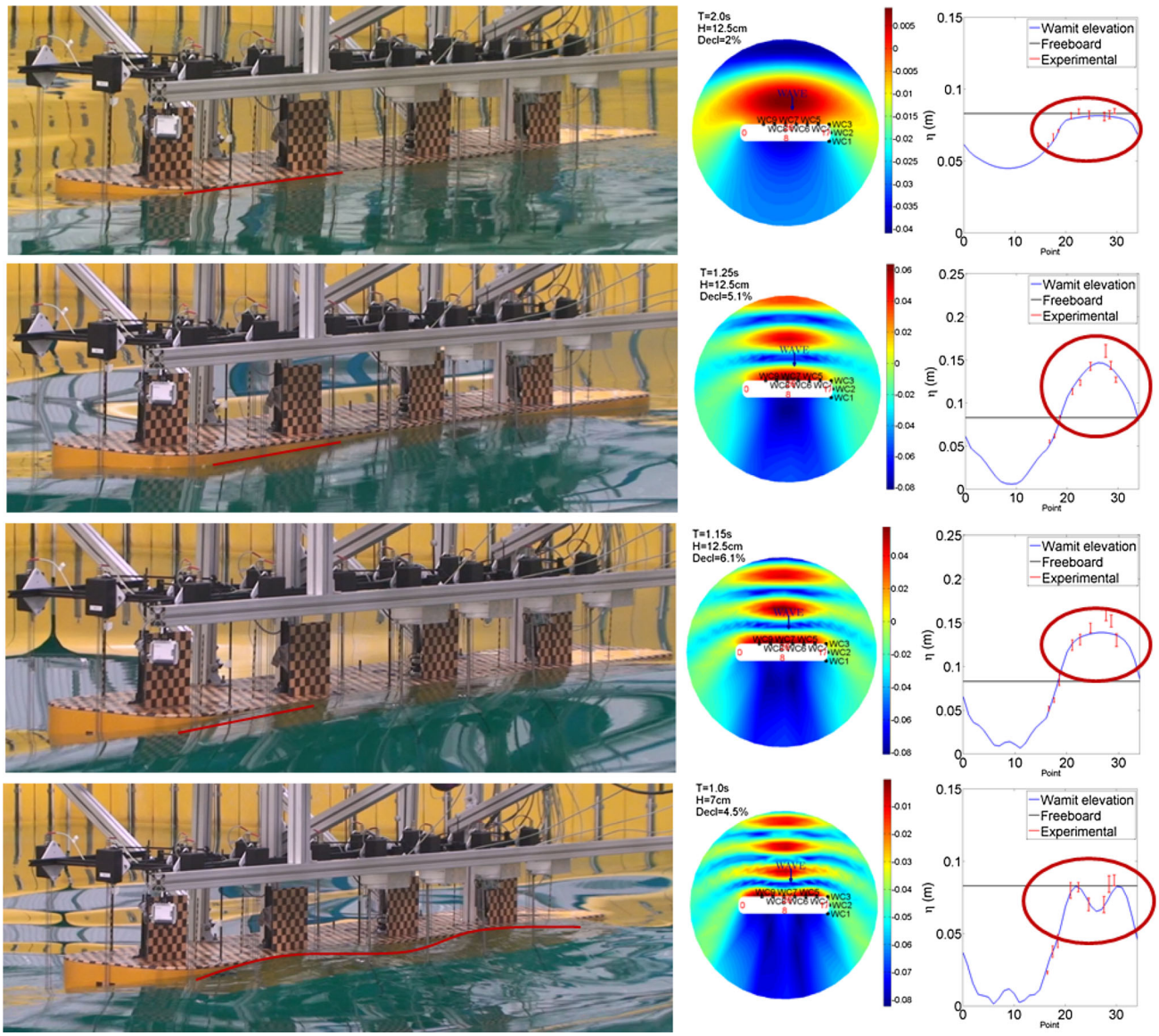


**Fig. 16** Comparison of free surface elevation for model scale wave period 1.0s (T=10.0 s, $\lambda = 156$ m—real scale), 1.15 s ($T = 11.5$ s, $\lambda = 206$ m—real scale), 1.25 s ($T = 12.5$ s, $\lambda = 244m$—real scale) and 2.0 s ($T = 20.0$ s, $\lambda = 625$ m—real scale) for heading 270, fixed model (Color figure online)

$\lambda = 244$ m—real scale) the surface elevation in the fore region is lower than the stern one, which could be also predicted by WAMIT calculations. On the other hand, for longer waves ($T = 2.00$ s, $\lambda = 6.25$ m—model scale/ $T = 20.0$ s, $\lambda = 625$ m—real scale) the opposite happens, obtaining higher elevations at the fore region compared with the stern one, as shown in Fig. 15. The agreement between potential theory predictions and experimental test is remarkable, which was unexpected for a simplified linear potential flow theory, mainly for high steepness waves.

Taking more attention to the recorded videos, it was verified that for the long waves the perturbation due to the

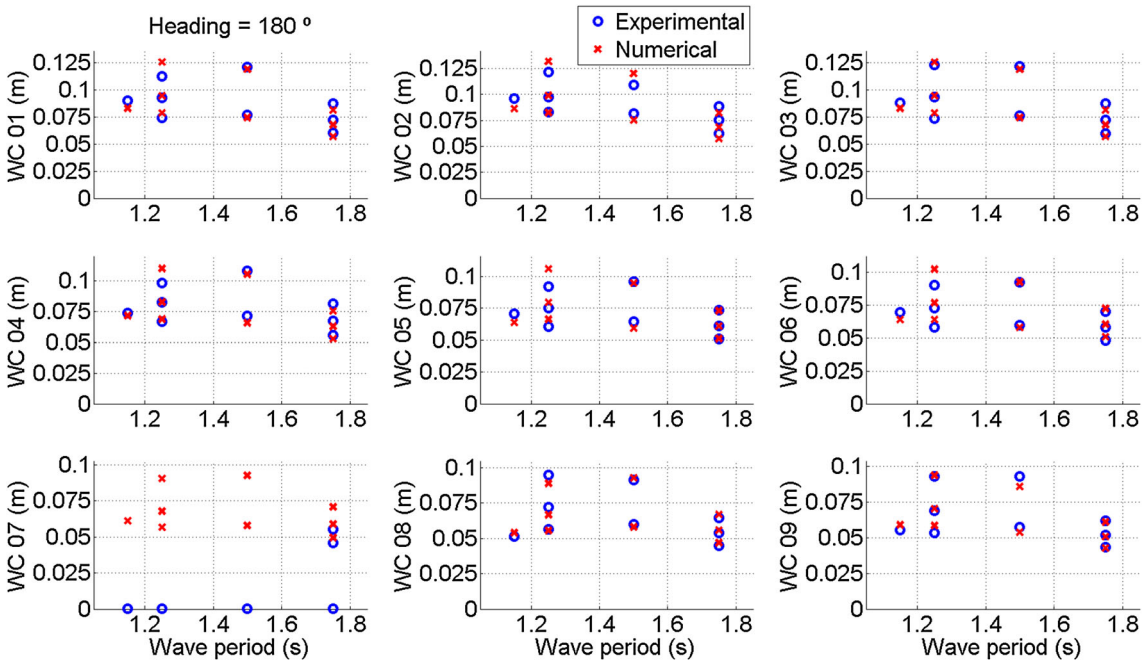


**Fig. 17** Comparison between experimental and numerical results for WC01-09 for 180 degrees heading

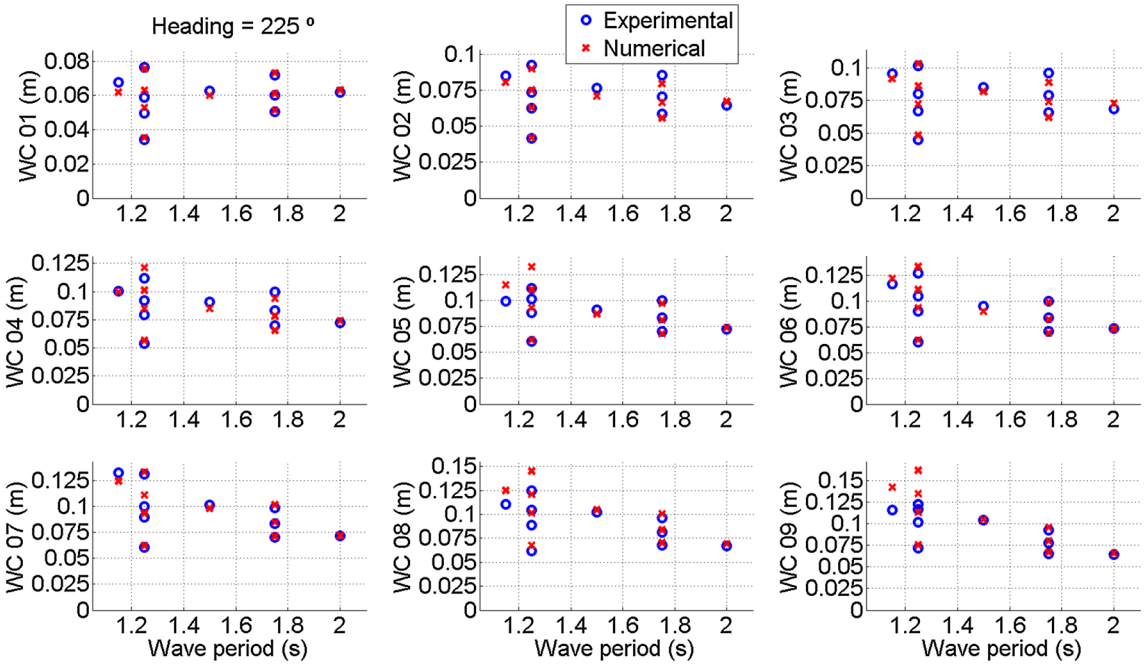


**Fig. 18** Comparison between experimental and numerical results for WC01-09 for 225 degrees heading

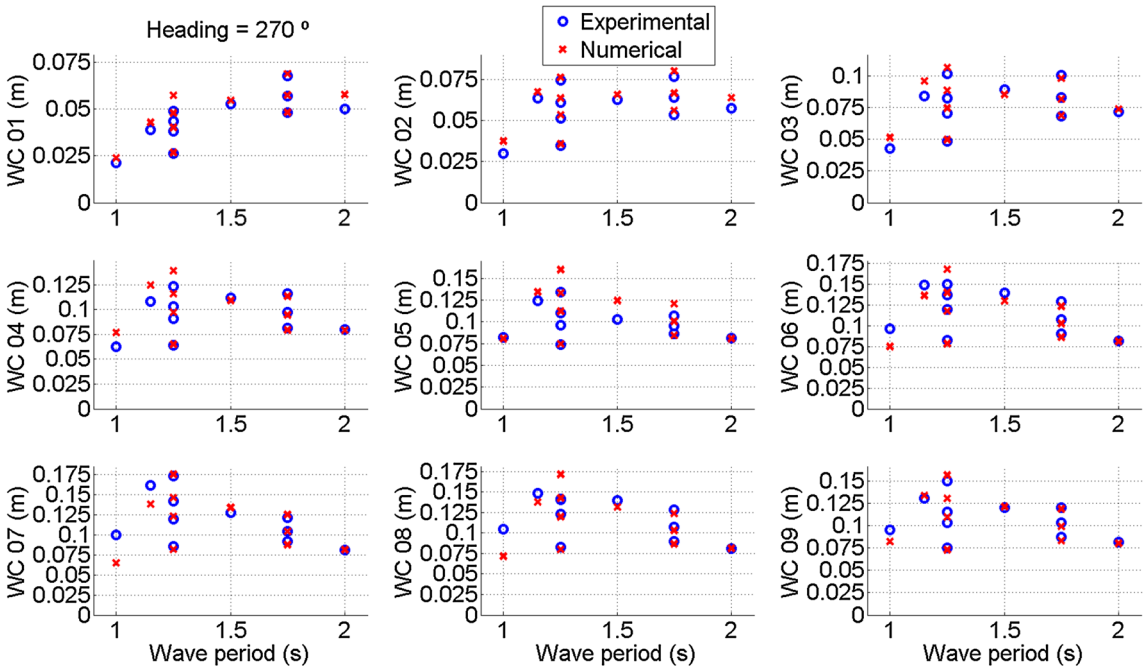


**Fig. 19** Comparison between experimental and numerical results for WC01-09 for 270 degrees heading

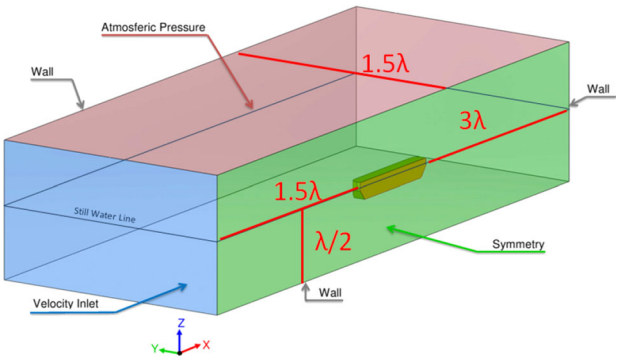


**Fig. 20** Computational domain assumed in the 180 heading simulation

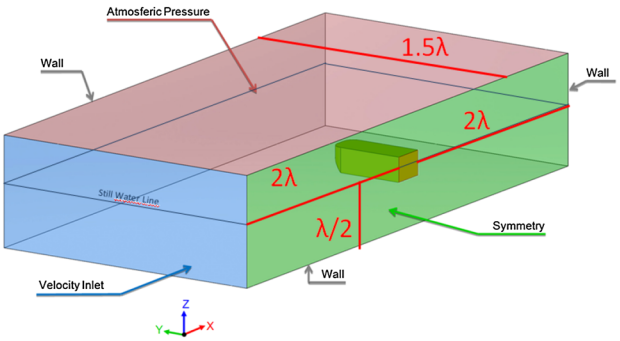


**Fig. 22** Computational domain assumed in the 270 heading simulation

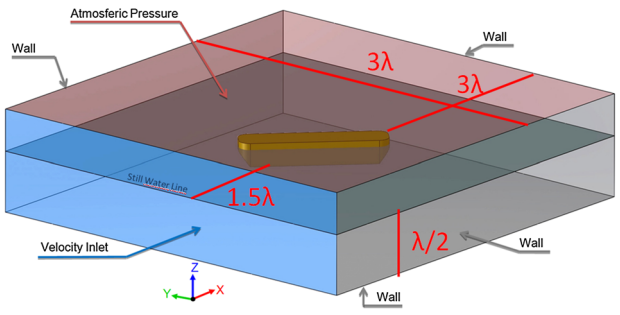


**Fig. 21** Computational domain assumed in the 225 heading simulation

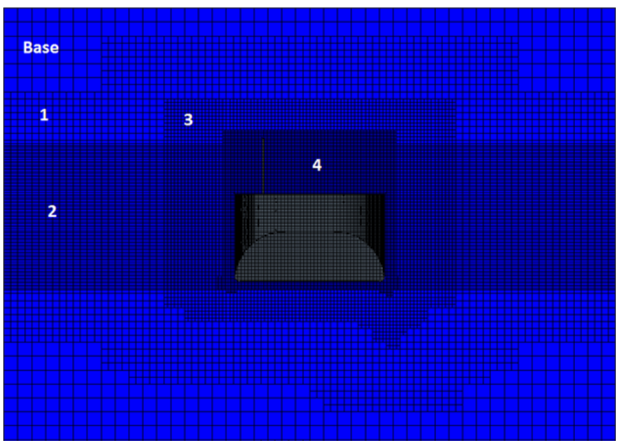


**Fig. 23** Details regarding the mesh refinement

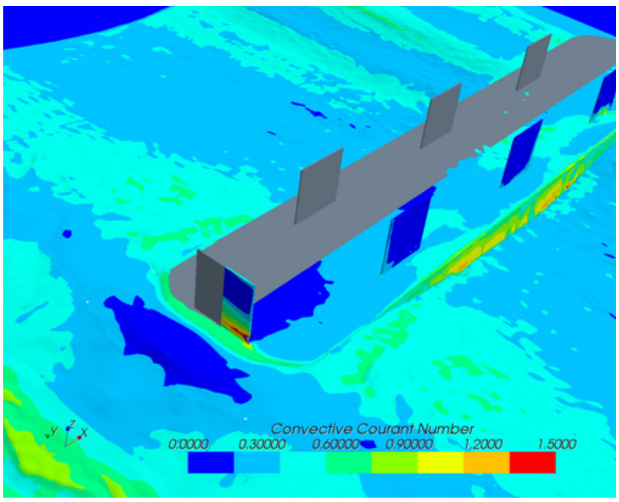


**Fig. 24** Example of Courant number distribution—180 heading (Color figure online)

hull is very small, reducing the elevation in the stern region, while for the short waves the hull acts as a barrier (almost an wall), inhibiting the wave to go through the hull (passing below the keel), so the wave "runs" in the sidehull and interacts constructively with the incident wave, increasing the elevation in the stern region. This fact is numerically reinforced because mean drift forces are maximum exactly in the range of 1.15 and 1.25s of wave period (model scale).

### *3.2.3 270 degrees heading*

The experimental tests considering beam sea conditions showed that for short waves, the diffraction due to the hull is very important, changing the free surface elevation pattern along the sidehull considerably depending on the wave period. It was verified that for waves around 1.0 s—model scale ($T = 10.0$ s, $\lambda = 156$ m—real scale)—the free surface pattern has a concentration of water around the ship shoulders while amidship the surface elevation is reduced. However, increasing the wave period to around 1.15 s—model scale ($T = 11.5$ s, $\lambda = 206$ m—real scale)—the free surface elevation becomes almost constant in the sidehull, providing an almost 2D flow. The free surface elevation for the 1.25-s wave period in model scale ($T = 12.5$ s, $\lambda = 244$ m—real scale) shows significantly 3D effects, with a large amount of water concentrated amidship, increasing the free surface elevation in this region compared with the fore and stern region.

On the other hand, for long waves, the free surface elevation acts as a wall of water that goes up similarly in the entire sidehull, reducing the variations between amidship and fore/stern regions. This behavior can be understood according to the long wave theory, which states that the wave diffraction due to a fixed/floating body reduces for increasing incident wave lengths.

This difference is illustrated in Fig. 16 considering 1.0-, 1.15-, 1.25- and 2.0-s wave periods (model scale), where it can be seen that for the longer wave the free surface

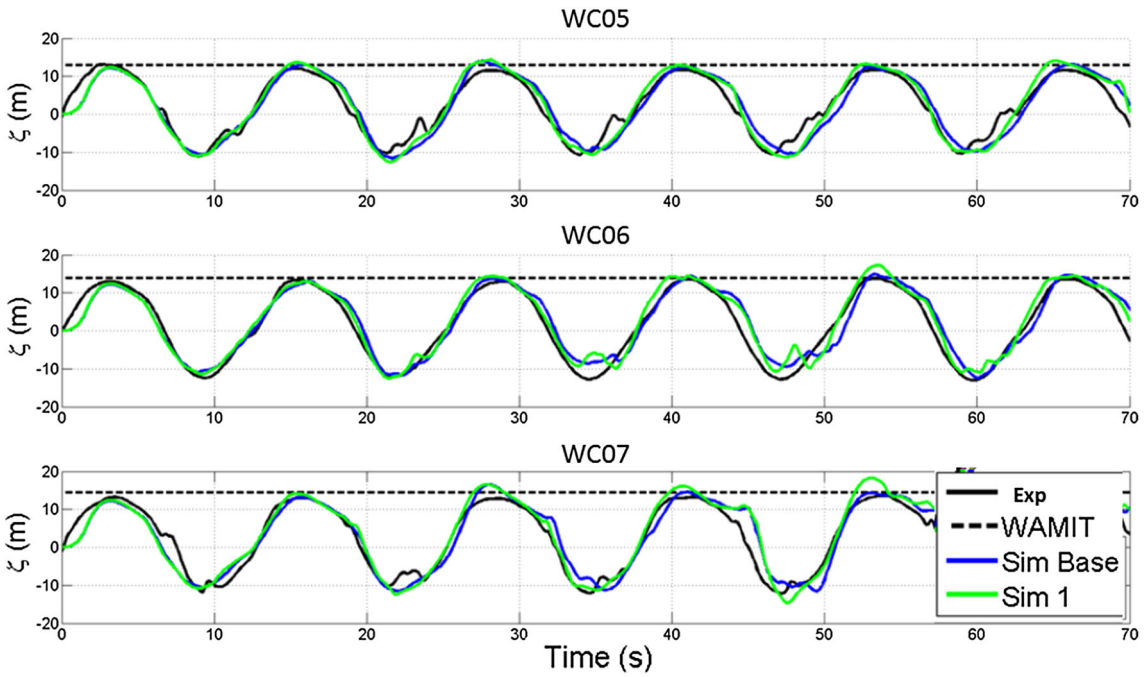


**Fig. 25** Mesh study—comparison of free surface elevation—Simulation 1 (Color figure online)

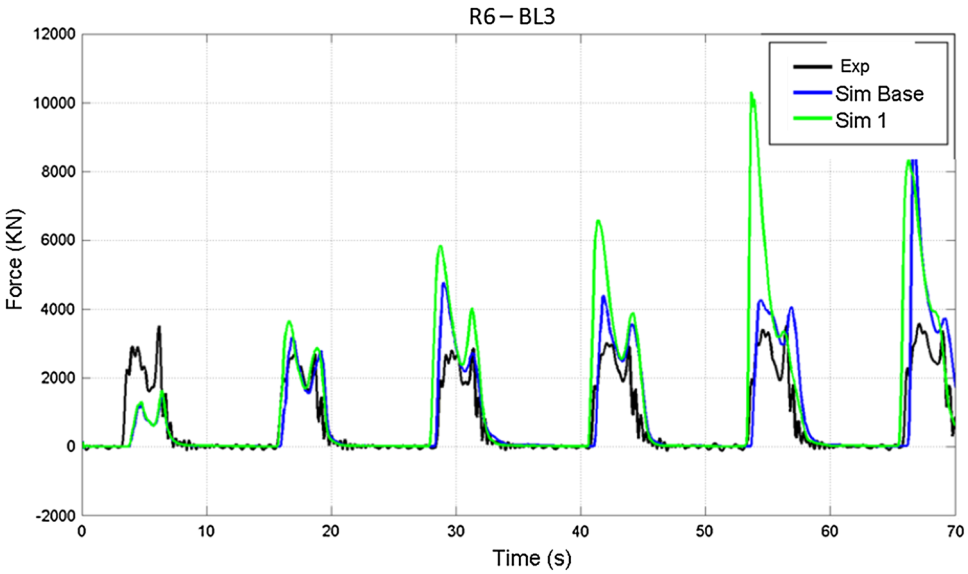


**Fig. 26** Mesh study—comparison of impact forces—Simulation 1 (Color figure online)

**Table 4** Simulated wave properties

| Heading | Wave | Hs (cm) | Tp (s) |
|---|---|---|---|
| 180 | Regular 8 | 15.0 | 1.25 |
| 180 | Regular 9 | 12.5 | 1.15 |
| 180 | Regular 11 | 20.0 | 1.50 |
| 180 | Regular 12 | 20.0 | 1.25 |
| 225 | Regular 6 | 12.5 | 1.25 |
| 225 | Regular 8 | 15.0 | 1.25 |
| 225 | Regular 9 | 12.5 | 1.15 |
| 270 | Regular 3 | 15.0 | 1.75 |
| 270 | Regular 4 | 12.5 | 1.50 |
| 270 | Regular 6 | 12.5 | 1.25 |
| 270 | Regular 7 | 10.5 | 1.25 |
| 270 | Regular 8 | 15.0 | 1.25 |
| 270 | Regular 9 | 12.5 | 1.15 |

elevation is almost constant around the entire sidehull, while for the shorter ones the pattern is significantly dependent on wave period. In order to verify the numerical capability in predicting this behavior, especially for the reduced wave periods, a comparison against WAMIT predictions was also included in the figure. It can be seen that the numerical method could reproduce the diffraction pattern near the hull very well, even for the smaller wave periods, providing a reliable "simple" method to predict the free surface elevation for this condition.

This conclusion regarding the beam sea condition is important because due to the FPSO geometry in a first analysis the flow could be considered as bidimensional. However, as verified experimentally the diffraction is completely tridimensional; therefore, the simulations using FVM should be performed considering the entire hull, instead only the midship section, which was discussed by [10].

The comparisons concerning all wave conditions for the wave probes can be summarized from Figs. 17, 18 and 19. It should be noticed that for some wave periods there are several free surface elevation values due to the several incident wave height. Besides, WC07 was not working properly for the head sea condition.

### 3.3 Forces comparison

The forces on the blocks located in the main deck were computed using StarCCM+ finite volume solver and compared with the experimental data available. The flow was modelled as laminar, assuming that the impact phenomenon as mostly influenced by inertial effects and the turbulence does not change the loads appreciably. The multiphase flow was evaluated using a VoF[5] approach, and an implicit temporal scheme was assumed to improve numerical stability. The coordinate system is located with its origin in the undisturbed free surface (plane XY) with the Z positive upward with the origin amidship. In the scope of this work, no damping zone was selected to damp the waves; therefore, the results can only be considered for some wave cycles without any influence of wave reflection.

#### *3.3.1 Domain dimensions and boundary conditions*

The domain dimension was defined to guarantee that during the simulation time the reflection effects would be

[5] Volume of fluid.

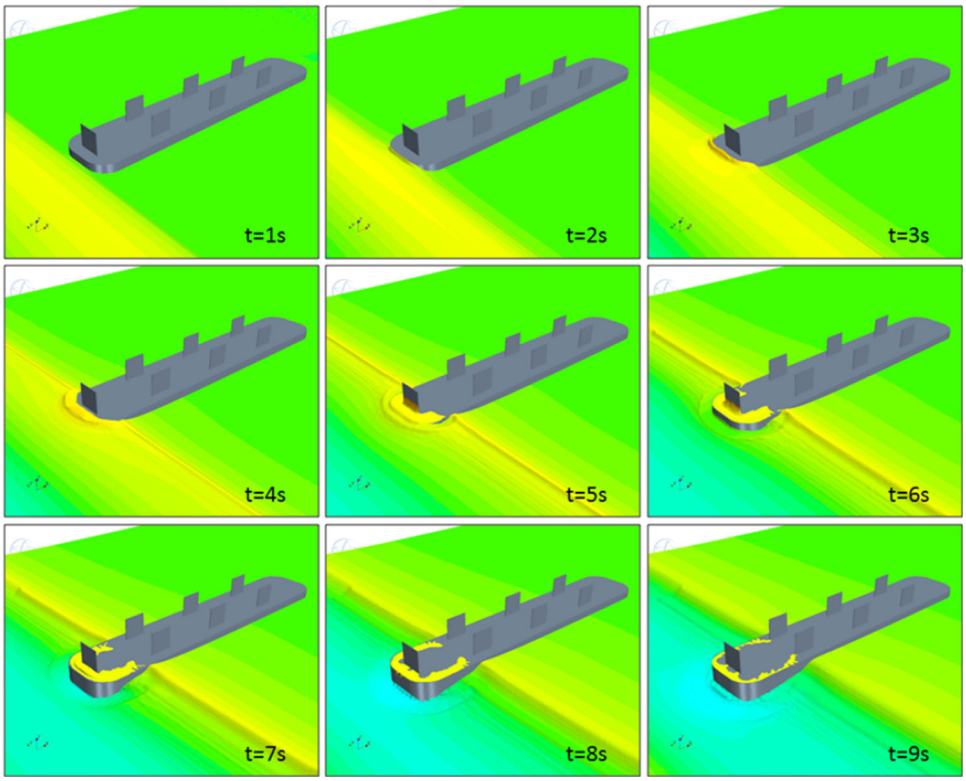


**Fig. 27** Wave propagation for wave R8 for 180 heading

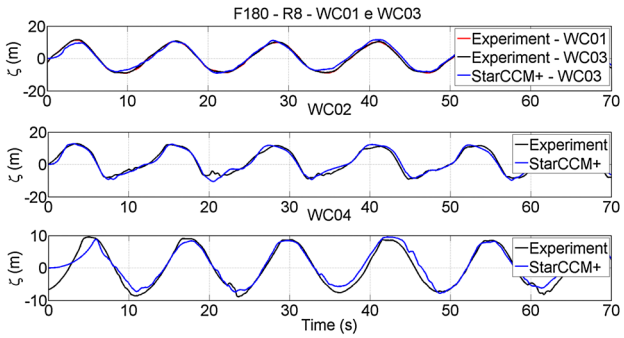


**Fig. 28** Comparison between numerical simulation and experimental data for WC01-WC04 for regular wave R8, 180 heading (Color figure online)

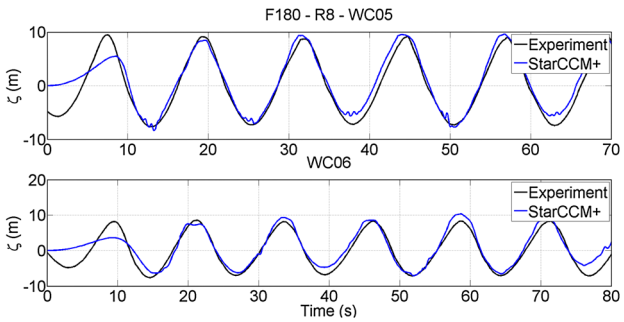


**Fig. 29** Comparison between numerical simulation and experimental data for WC05-WC07 for regular wave R8, 180 heading (Color figure online)

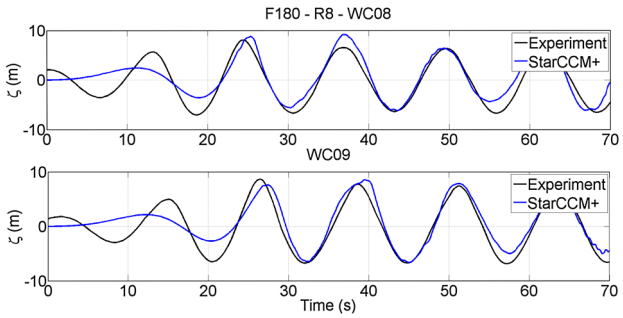


**Fig. 30** Comparison between numerical simulation and experimental data for WC08-WC09 for regular wave R8, 180 heading (Color figure online)

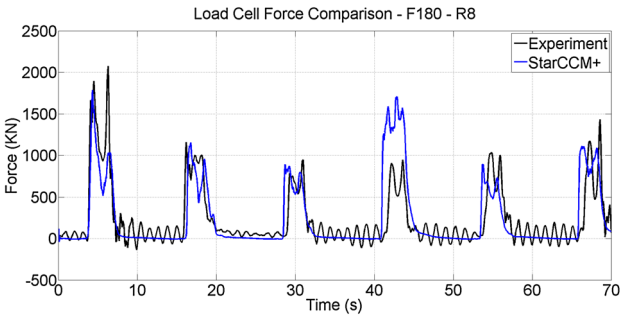


**Fig. 31** Comparison between numerical simulation and experimental data for impact block 01 for regular wave R8 under 180 heading (Color figure online)

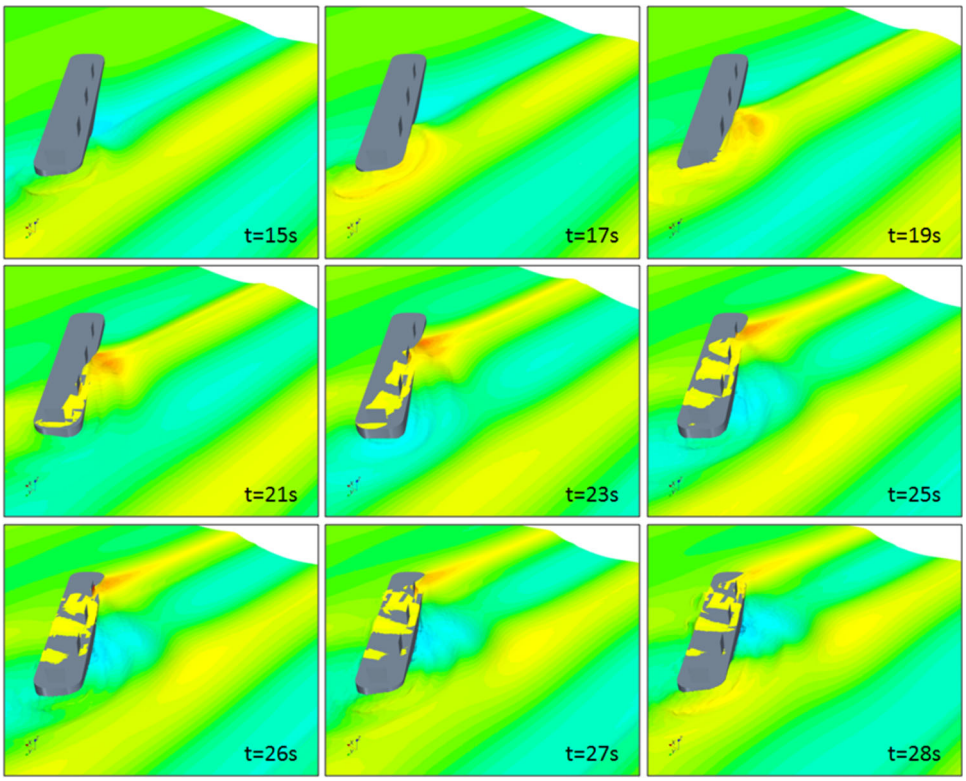


**Fig. 32** Example of wave propagation for wave R8 for 225 heading

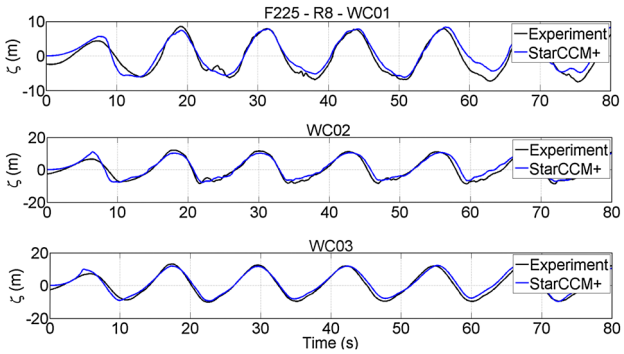


**Fig. 33** Comparison between numerical simulation and experimental data for WC01-WC03 for regular wave R8, 225 heading (Color figure online)

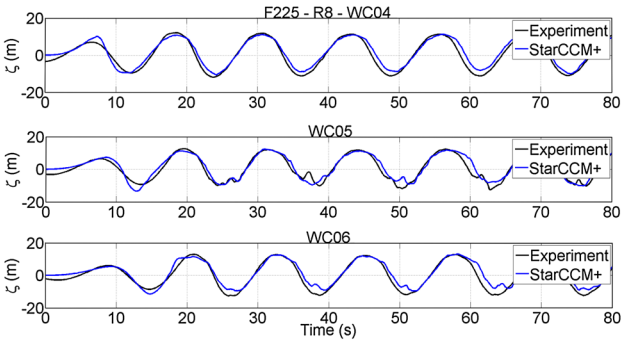


**Fig. 34** Comparison between numerical simulation and experimental data for WC04-WC06 for regular wave R8, 225 heading (Color figure online)

negligible, assuming the linear wave propagation theory to compute the wave group velocity and define the theoretical reflection time, assuming the vessel as wall that would reflect the waves completely. Since wave length and velocity are period dependent for each wave condition, the domain was built to keep the same number of cycles.

The boundary conditions and dimensions assumed in the numerical model are summarized in Figs. 20, 21 and 22, where $\lambda$ is the wave length, considering a velocity inlet with a linear wave velocity profile in the generation boundary, walls[6] in the remaining boundaries (free slip in all boundaries but the body, where a no slip condition was assumed) and a pressure outlet in the top with atmospheric value assumed.

### 3.3.2 Mesh generation

The mesh was built using hexaedric elements following a multiblock approach, considering several refinement blocks in the regions where the flow is more complex or required a better description, see for instance the deck region in Fig. 23, providing a 10-M cell mesh. An

[6] Actually a symmetry condition is imposed in the symmetry plane, which is basically the same as free slip wall condition.

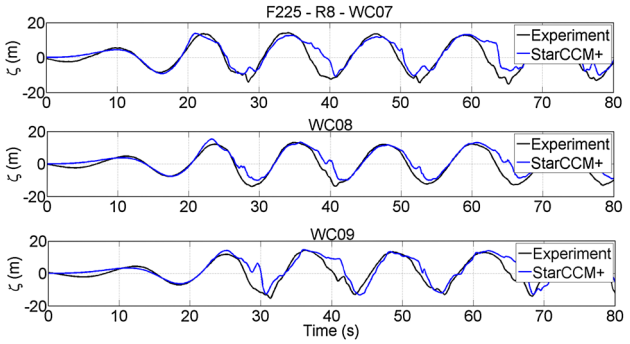


**Fig. 35** Comparison between numerical simulation and experimental data for WC07-WC09 for regular wave R8, 225 heading (Color figure online)

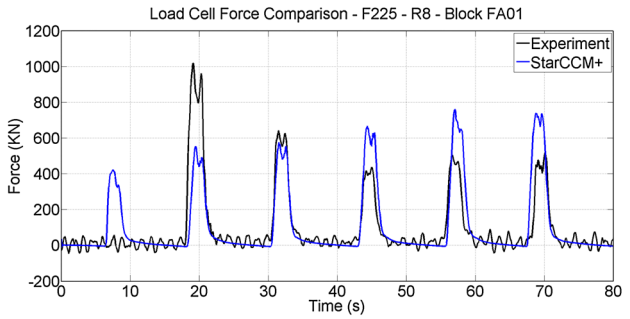


**Fig. 36** Comparison between numerical simulation and experimental data for impact block 01 for regular wave R8 under 225 heading (Color figure online)

additional refinement block was added around the undisturbed free surface interface to capture the wave propagation.

### 3.4 Mesh optimization and convergence

The simulation was solved assuming a second-order discretization in time with a time step of 0.05 s and 20 inner iterations. The block structured mesh combined with this time step could produce dimensional residues of less than $2.0 \times 10^{-4}$ concerning all equations and an averaged Courant number of 0.5, with maximum values of about 1.5 in specific instants of the simulation and some critical points of the domain (close to the impact points—see Fig. 24).

In order to reduce the number of elements in the simulation, the mesh configuration was investigated concerning element size and refinement block positioning.[7] Since the simulation is unsteady, the time step will also influence

[7] Since the mesh is built as multiblock, the base size parameter can be used to verify mesh convergence after a refinement block distribution is defined.

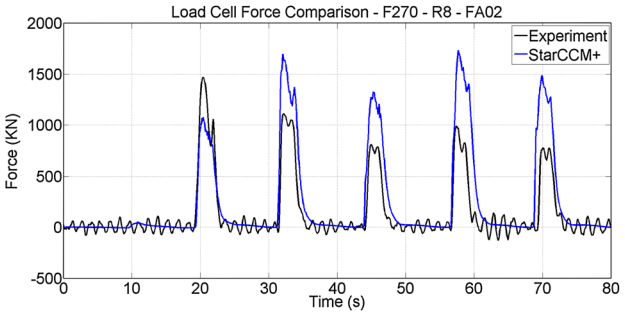


**Fig. 37** Comparison between numerical simulation and experimental data for impact block 02 for regular wave R8 under 225 heading (Color figure online)

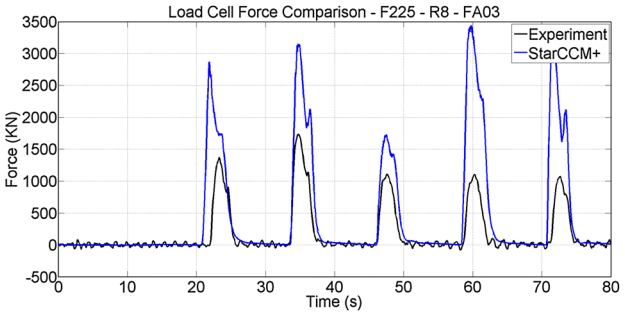


**Fig. 38** Comparison between numerical simulation and experimental data for impact block 03 for regular wave R8 under 225 heading (Color figure online)

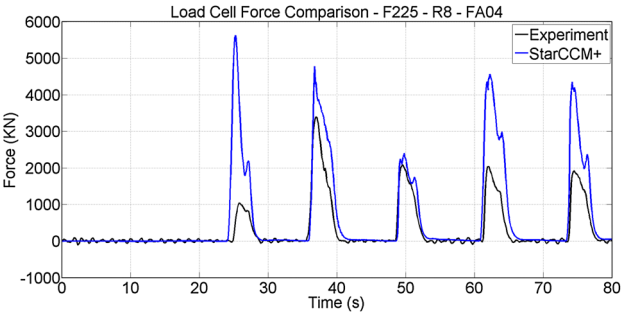


**Fig. 39** Comparison between numerical simulation and experimental data for impact block 04 for regular wave R8 under 225 heading (Color figure online)

the results; therefore, two values were tested to verify the differences.

The regular wave 6 was chosen in the study (Tp = 1.25 s e Hs = 12.5 cm), and the results were compared with the experimental data for a setup with a mesh of 10-M elements (time step 0.015 s) and 5.7-M elements (time step of 0.030 s) concerning free surface elevation in the sidehull (WC05, WC06 e W07) and forces in the impact block located amidship (BL03) for beam sea conditions.

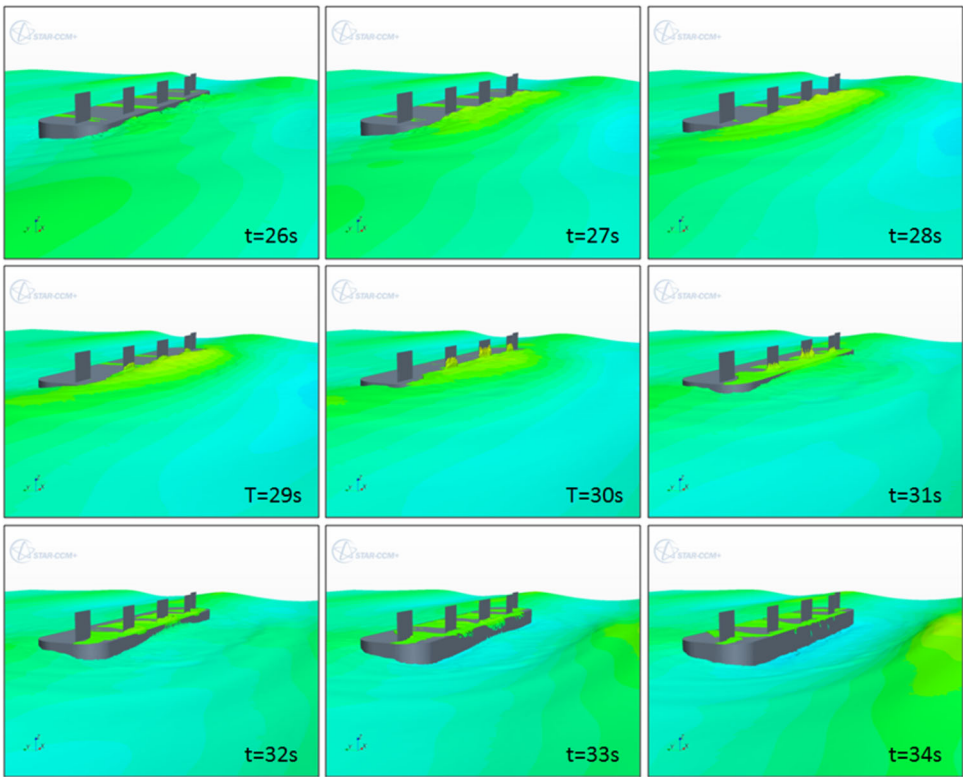


**Fig. 40** Example of wave propagation for wave R6 for 270 heading

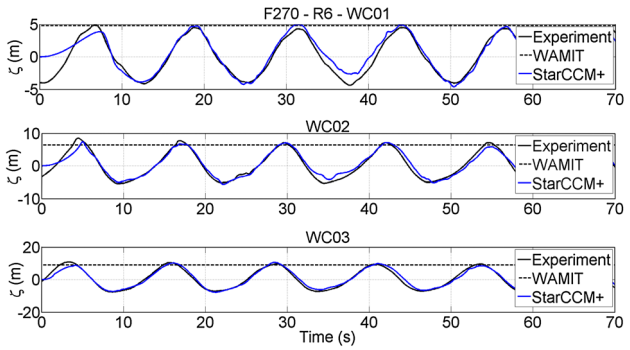


**Fig. 41** Comparison between numerical simulation and experimental data for WC01-WC03 for regular wave R6, 270 heading (Color figure online)

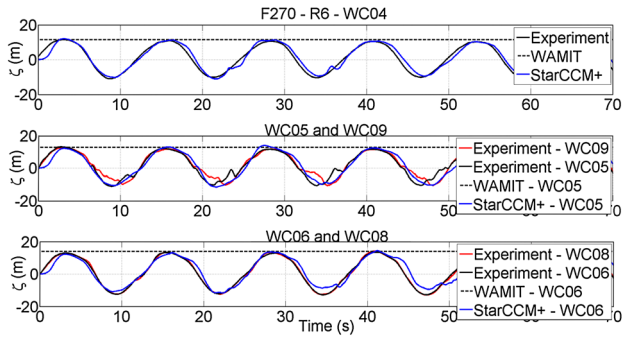


**Fig. 42** Comparison between numerical simulation and experimental data for WC04-WC09 for regular wave R6, 270 heading (Color figure online)

The differences concerning the Simulation 1 and the base simulation are in the mesh structure, since Simulation 1 setup was generated with the refinement blocks closer to the impact block reducing the number of elements compared with the base one. The comparison of the results can be seen in Figs. 25 and 26 concerning free surface elevation and forces on the block, respectively. It can be seen that although the free surface elevation had almost no significant changes, the impact force peaks are significantly different, which could be explained by the nonlinear influence of the velocity field.

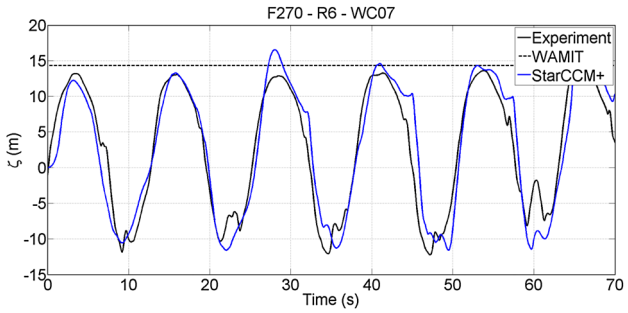


**Fig. 43** Comparison between numerical simulation and experimental data for WC07 for regular wave R6, 180 heading (Color figure online)

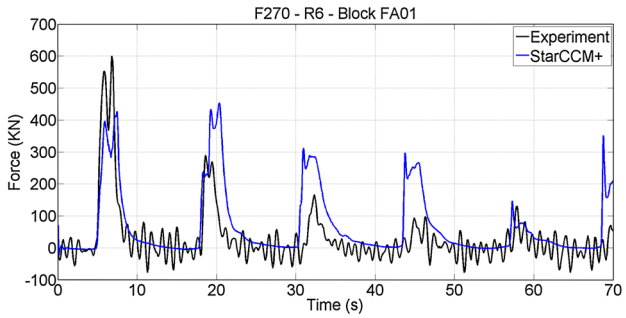


**Fig. 44** Comparison between numerical simulation and experimental data for impact block 01 for regular wave R6 under 270 heading (Color figure online)

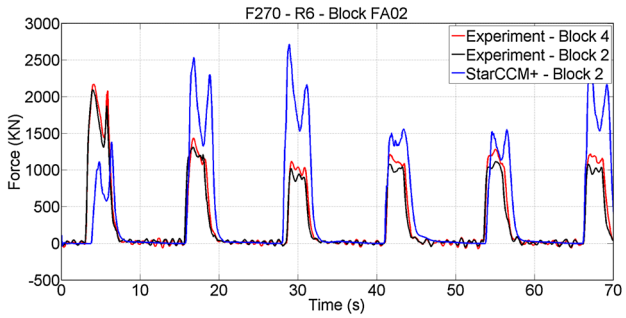


**Fig. 45** Comparison between numerical simulation and experimental data for impact block 02 for regular wave R6 under 270 heading (Color figure online)

The wave conditions shown in Table 4 were simulated using the setup presented earlier, since these waves provided severe green water events according to experimental observations.

The comparison is performed considering the wave probes located in the sidehull (WC01-WC09) and force series in the impact blocks, always having in mind the symmetry hypothesis assumed in the 180 and 270 heading. However, since in the 180 heading only the impact block BL01 is perpendicular to the wave propagation direction, the only meaningful measurements are provided by this block. The results are converted to real scale assuming Froude similarity (Fig. 27).

An example of comparison between experimental data and numerical simulations concerning free surface elevation and forces in the impact block can be seen in Figs. 28, 29, 30 and 31. A good agreement could be found between the results, and the high fluctuations in the results were assumed as related to a stochastic process that should be described using some statistics, as should be investigated in further studies .

The 225° green water events are quite different than the 180 heading, and for some wave periods the impacts are much more severe in the stern region than in the fore one as

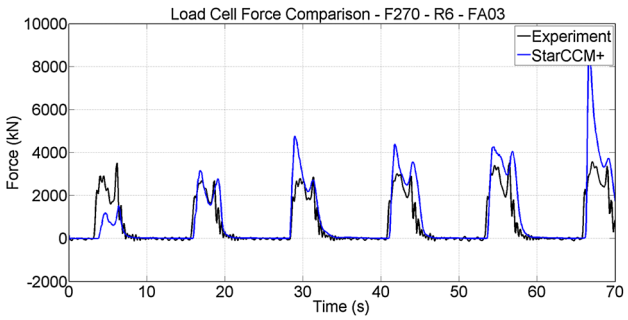


**Fig. 46** Comparison between numerical simulation and experimental data for impact block 03 for regular wave R6 under 270 heading (Color figure online)

illustrated, for example, in Fig. 32. This fact is also verified experimentally (Figs. 33, 34, 35); however, the forces predicted by the numerical method are reasonably higher than the experimental data, which can be considered as good from an engineering point of view, as can be seen in Figs. 36, 37, 38 and 39 (Fig. 40).

The comparisons concerning 270 heading can be seen in Figs. 41, 42, 43, 44, 45 and 46, and a good agreement was found between numerical prediction and experimental data. It should also be noticed that there is a significant variability in the results concerning maximum impact forces.

## 4 Conclusions

From the results obtained both numerically and experimentally for the captive vessel, it can be concluded that wave periods are a key driver to wave run-up along the hull and the physics concerning the water overtopping changes according to the platform heading. In head seas the critical point for water on deck is the bow regardless wave period, while for bow-quartering condition the critical position changes according to the wave period with the bow as the most susceptible region for long waves and stern for short ones.

In the case of beam sea condition, the critical points change according to the period; therefore, for the longest waves (2.0 s) the relative elevation is a little more severe amidship than in the shoulders and these differences increase by reducing wave period to 1.25 s. However, by reducing the wave period to 1.15s the relative elevation amidship is equal to the shoulder regions, and reducing the period even more (to 1.0 s) the relative elevation is bigger in the shoulder region than amidship. It should also be noticed that all these trends could be computed using WAMIT first-order potential solution. The accuracy of the numerical method to obtain the maximum elevations even for high steepness waves is remarkable.

In this sense and taking into account the efficiency of the numerical method, this methodology could be extended to free-floating simulations and then be applied to the entire metocean of Santos Basin to define the critical sea states in terms of relative elevation, which will be the next steps in the study.

**Acknowledgments** The authors would like to thank Petrobras for the support provided during this research.

## References

1. B. Buchner, Green water on ship-type offshore structures. PhD thesis, Delft University (2002)
2. B. Buchner, J.L. Cozijn, An investigation into the numerical simulation of green water, in *Proceedings of International Conference on Behaviour of Offshore Structures, BOSS'97,* Delft, vol. 2 (1997), pp. 113–125
3. W.E. Cummins, The impulse response and ship motions. Technical report, Department of the Navy David Taylor Model Basin (DTMB) (1962)
4. Incorporation W, Wamit users manual v 7.0 (2013), http://www.wamit.com
5. R.L. Leonhardsen, G. Ersdal, A. Kvitrud, Experience and risk assessment of FPSOs in use on the norwegian continental shelf descriptions of events, in *Proceedings of the 11th International Conference on Offshore and Polar Engineering* (2001)
6. P.C. Mello, M.L. Carneiro, E.A. Tannuri, K. Nishimoto, Usp active absorption wave basin from conception to commissioning, in *Proceedings of the ASME 2010 29th International Conference on Ocean, Offshore and Arctic Engineering* (2010)
7. F. Ruggeri, A time domain rankine panel method for 2D seakeeping analysis. PhD thesis, University of São Paulo (2012)
8. R.V. Schiller, C. Pakozdi, D.G.T. Yuba, C.T. Stansberg, D.F.C. Silva, Green water on FPSO predicted by a practical engineering method and validated against model test for irregular waves, in *Proceedings of the ASME 33rd International Conference on Ocean, Offshore and Arctic Engineering, OMAE2014-23084* (2014)
9. T. Schoember, R.C.T. Rainey, A hydrodynamic model of green water incidents. Appl. Ocean. Res. **24**(5), 299–307 (2002). doi:10.1016/S0141-1187(03)00004-X
10. D.F.C. Silva, R.R. Rossi, Green water loads determination for FPSO exposed to beam sea conditions, in *Proceedings of the ASME 33rd International Conference on Ocean, Offshore and Arctic Engineering, OMAE2014-24947* (2014)
11. C.T. Stansberg, K. Berget, A simple tool for prediction of green water and bow flare slamming on FPSO, in *Proceedings of the ASME 2009 28th International Conference on Ocean, Offshore and Arctic Engineering* (2009)
12. E.F.G. van Daalen, Numerical and theoretical studies of water waves and floating bodies. PhD thesis, University of Twente (1993)
13. Z.Q. Zhou, J.O. De Kat, B. Buchner, A nonlinear 3-D approach to simulate green water dynamics on deck, in *Proceedings of the 7th International Conference on Numerical Ship Hydrodynamics* (1999)